LAWRENCE
LIVERMORE
NATIONAL
LABORATORY

LLNL-JRNL-464111

Diesel Engine Dynamometer Testing of Impedancemetric NOx Sensors

L. Y. Woo, R. S. Glass, R. F. Novak, J. H. Visser

December 16, 2010

Sensors and Actuators B: Chemical

Disclaimer

Diesel Engine Dynamometer Testing of Impedancemetric NO_x Sensors

L.Y. Woo[a,], R.S. Glass[a], R.F. Novak[b], J.H. Visser[b]

[a] *Lawrence Livermore National Laboratory, Livermore, California 94551, USA*
[b] *Ford Motor Company, Dearborn, Michigan 48121, USA*

Abstract

Prototype solid-state electrochemical sensors using a dense gold sensing electrode, porous yttria-stabilized zirconia (YSZ) electrolyte, and a platinum counter electrode (Au/YSZ/Pt) were evaluated for measuring NO_x (NO and NO_2) in diesel exhaust. Both electrodes were exposed to the test gas (i.e., there was no reference gas for the counter electrode). An impedancemetric method was used for NO_x measurements, where the phase angle was used as the response signal. A portion of the tailpipe exhaust from the dynamometer test stand was extracted and fed into a furnace containing the experimental sensor. The prototype sensor was tested along with a commercially available NO_x sensor. Simultaneous measurements for NO_x, O_2, CO_2, H_2O, CO, and CH_4 in a separate feed stream were made using Fourier transform infrared (FTIR) spectroscopy and an oxygen paramagnetic analyzer. The experimental sensor showed very good measurement capability for NO in the range of 25-250 ppm, with a response paralleling that of the FTIR and commercial sensor. The prototype sensor showed better sensitivity to NO_x at the lower concentration ranges. O_2 is an interferent for the experimental sensor, resulting in decreased sensitivity for measurement of NO_x. Methods to overcome this interference are discussed.

Keywords: NO_x; Exhaust gas sensor; Electrochemical sensor; Impedancemetric sensor

1. Introduction

Compared to gasoline internal combustion engines, diesel engines emit smaller amounts of carbon monoxide, hydrocarbons, and carbon dioxide, and are readily adaptable for renewable fuels such as biodiesel. However, additional exhaust after treatment and engine optimization are needed to meet all the emission regulations, especially for NO_x, NO and NO_2. Advanced NO_x sensors are being developed for use in feedback control systems to reduce emissions [1–4]. Along with challenging technical performance requirements for stability, accuracy, and sensitivity, the cost of sensors is also an important issue [5–7]. Solid-state electrochemical sensors, like the oxygen stoichiometric sensor, are proven technology for the harsh high-temperature environment in automotive exhaust [3–7].

To the authors' knowledge, at this time there exists only one commercial technology, which uses yttria-stabilized zirconia (YSZ) as the oxygen-ion conducting electrolyte and a dual chamber design. The first chamber functions as an electrochemical pump to remove oxygen, which interferes with the measurement of NO_x. The sampled gas is then passed into a second chamber where the measurement of NO_x takes place. The NO_x measurement is made amperometrically by applying a voltage to the electrochemical cell in the second chamber and measuring the currents associated with the reduction of NO_x at the sensing electrode. However, the currents corresponding to ppm levels of NO_x, which is the desired sensitivity to meet future regulations, are extremely small and on the order of nanoamps. The dual chamber design and associated electronics necessary to allow measurement of extremely low concentrations of NO_x make this sensor complex and costly. It is doubtful that it can meet 2015 Tier 2, Bin 8 requirements in terms of sensitivity (single ppm level NO_x), or that the cost of this sensor can be reduced enough to meet automobile manufacturer goals. Consequently, a new type of NO_x sensor is desired.

Prior work has investigated solid-state electrochemical sensors for NO_x based on yttria-stabilized zirconia (YSZ) electrolyte and an impedancemetric (sometimes referred to as impedimetric) sensing approach [9–15]. In contrast to the dc

measurements made using amperometric (where current is measured and related to NO_x concentration) or potentiometric (where voltages are measured and related to NO_x concentration) approaches, the impedancemetric approach uses ac measurements at a specified frequency. This method of operation has shown the potential for higher sensitivity towards NO_x, better long-term stability, and lower cost materials [12–15].

The approach is related to solid-state impedance spectroscopy, an electrochemical characterization technique that measures the electrochemical cell response over a range of frequencies, typically from subhertz to megahertz [16]. The frequency-dependent behavior can be used to identify individual electrochemical components if they have significantly different time constants (e.g., interfacial and bulk phenomena), in which case they can be separated for individual analysis. The electrode impedance or polarization, primarily associated with processes at the electrode/electrolyte interface, dominates the low frequency regime, typically at less than 1 kHz. The response at low frequencies is related to the NO_x concentration since electrochemical reactions involving NO_x dominate the interfacial processes in this regime. The interested reader is directed to other sources for a complete description of this method, Refs. [13–15].

In this work we use a prototype Au/YSZ/Pt sensor to measure the impedancemetric response in diesel engine exhaust. The results are compared to a commercially available NO_x sensor and measurements of gas composition using Fourier-transform infrared spectroscopy and a paramagnetic oxygen analyzer. The effect of oxygen on the NO_x response is evaluated.

2. Material and methods

Preparation of the NO_x sensor prototype has been described previously [15]. The prototype used a dense alumina substrate (99.6% Al_2O_3, 10 mm x 10 mm x 0.5 mm, Valley Design Corp.). Platinum ink (Engelhard 6082) was applied to the substrate and fired at 1200°C. A slurry of yttria-stabilized zirconia (YSZ) powder (Tosoh Corp., 8 mol% Y_2O_3-doped ZrO_2) mixed with ethanol,

binder (polyvinyl butyral, Butvar), dispersant (phosphate ester), and plasticizer (dipropylene glycol dibenzoate) was then applied on top of the fired Pt. Au wire (0.25 mm diameter, Alfa Aesar) electrodes were wrapped around the entire substrate with additional YSZ slurry applied on top of the wires. The assembled prototype was fired at 1000°C. Figure 1 shows a schematic of the Au wire NO_x sensor prototype. Additional ceramic adhesive (Ultra-Temp 516, Aremco Products, Inc.) was applied along the edges to secure the Au wire electrodes to the alumina substrate.

Laboratory gas sensing experiments were performed in a quartz tube (21.4 mm I.D.) placed inside a tube furnace with both electrodes exposed to the same environment. Gas composition was controlled by mixing air, N_2, and a 1000 ppm NO/NO_2 feed using a standard gas handling system equipped with thermal mass flow controllers. The total gas flow rate was fixed at 500 ml/min. Water concentration was controlled to approximately 2% by flowing mixtures of air and N_2 through a water bubbler and combining with dry mixtures of N_2, NO and NO_2, which prevented NO_x from dissolving in the water. Measurements were performed at 650°C.

Dynamometer testing of diesel exhaust was performed at Ford Research Center using an engine test cell with engine gas recirculation (EGR) and urea-based selective catalytic reduction (SCR) system for reducing NO_x emissions. A portion of the tailpipe exhaust was extracted and fed into a furnace containing the prototype sensor. Due to variations in the exhaust gas flow rate for different engine conditions, temperature fluctuations in the furnace were monitored using a thermocouple located near the sensor prototype. Measured temperatures ranged from approximately 650 to 670°C. A commercial NO_x sensor was located downstream of the prototype.

Sensor performance data in tailpipe exhaust were obtained using a constant engine speed of 2750 rpm, and the exhaust gas composition was altered using variations in either the rate of urea injection in the SCR system or the percent throttle in the EGR. The exhaust gas composition, including CH_4, NO, NO_2, NH_3, CO, CO_2, and H_2O, was determined using Fourier transform infrared

(FTIR) spectroscopy, and O_2 concentration was determined using a paramagnetic oxygen analyzer.

A flow diagram of the dynamometer test setup is shown in Fig. 2. Two different protocols were used for the engine test. The first protocol involved constant throttle operation while stepping through different rates of urea injection, while the second protocol involved a fixed amount of urea injection while stepping through different amounts of throttle.

Laboratory electrochemical measurements were performed using a Solartron 1260 Impedance Analyzer in combination with a Solartron 1287 Electrochemical Interface, while engine testing at Ford used a stand-alone Solartron 1260 Impedance Analyzer. Computer-controlled data acquisition used the commercially available ZPlot software (Scribner Associates, Inc.). Impedance spectra were obtained using an excitation voltage of 25 mV over the frequency range 1 MHz to 1 Hz at 10 steps per frequency decade.

3. Results and discussion

Impedancemetric sensing has been described previously [12–15]. Briefly, impedance describes how the system responds to an applied alternating (ac) signal, and includes both magnitude, $|Z|$, and phase angle, θ, information. The complex impedance, $Z(\omega)$, is composed of both a real, Re(Z), and imaginary, Im(Z), component [16].

Either the magnitude or the phase angle of an impedancemetric response at a specified frequency can be used as the sensor signal [12–15]. In general, the phase angle has been found to exhibit better stability than the magnitude. Therefore, the phase angle parameter was used as the sensing signal to evaluate the performance of the NO_x sensor prototype.

3.1. Laboratory bench testing

Prior to testing in diesel engine dynamometer exhaust, bench-level laboratory testing of the sensor was conducted with controlled O_2 and NO_x concentrations. Figure 3 shows the a complex plane representation of -Im(Z) vs. Re(Z),

or Nyquist plot, for the Au/YSZ/Pt prototype at 650°C. The flowing gas contained about 2% H_2O and the prototype sensor response is shown in 10.5% O_2 and in 10.5% O_2 with either 100 ppm NO or 100 ppm NO_2. Each datum is taken at a different frequency, increasing from right to left, where the numbers corresponding to darkened points represent log of frequency in Hz.

In Fig. 3, the impedance of the prototype, in the frequency range of less than about 1 kHz, decreased when either NO or NO_2 were added. The addition of NO_2 caused a slightly larger decrease in impedance than NO, and at frequencies greater than about 10 kHz, the addition of NO_x had no apparent effect. Impedance changes at frequencies less than about 1 kHz are often attributed to electrode impedance, which depend on reactions at the interface between the electrode and electrolyte.

Figure 4a shows sensing behavior of the prototype using phase angle, in degrees, at 10 Hz and 25 mV excitation as the signal. Data were taken at 650°C in 10.5% O_2 and ∼2% H_2O. The NO concentration was then adjusted in two-minute steps starting with baseline (0 ppm NO). The concentration was stepped to 100, 50, and 20 ppm, then stepped in 5 ppm increments to 0 ppm and back to 20 ppm, and then stepped to 50 and 100 ppm before returning to baseline. All changes, including the 5 ppm increments, are clearly resolved.

Figure 4b shows the phase angle signal vs. NO concentration corresponding to the data shown in Fig. 4a. In Fig. 4b, the phase angle signal behavior was approximated using two separate linear regimes, one at low NO concentrations (0 to 20 ppm), and another at high NO concentrations (50 to 100 ppm). The sensitivity at low NO concentrations, as indicated by the slope (m_{low}), is ∼0.05 deg/ppm NO, while the sensitivity decreased at high NO concentrations (m_{high}) to ∼0.03 deg/ppm NO.

To investigate the effect of O_2 interference, bench-level laboratory testing also included measuring the phase angle response of the sensor over a range of O_2 concentrations. Data were taken at 650°C in about 2% H_2O for 4, 7, 10.5, and 12.6% O_2. The phase angel signal vs. O_2 concentration is shown in Fig. 5. Similar to the behavior in Fig. 4b, the behavior in Fig. 5 was also approximated

using two separate linear regimes, one at low O_2 concentrations (4 to 7%), and another at high O_2 concentrations (10.5 to 12.6%). The sensitivity at low O_2 concentrations, as indicated by the slope (m_{low}), is ~2 deg/% O_2, while the sensitivity decreased at high O_2 concentrations (m_{high}) to ~0.7 deg/% O_2.

3.2. Engine testing: isolating the effect of NO_x

After bench-level laboratory testing, the same NO_x prototype sensor was then evaluated by routing a portion of the tailpipe exhaust, from the engine dynamometer test cell, into a furnace. Two different protocols were used for the engine test. The first protocol allowed the effect of NO_x to be isolated by minimizing the effect of potential interferences, while the second protocol investigated the effect of O_2 cross-senstivity.

In the first protocol, to isolate the effect of NO_x, the engine was initially operated under a constant throttle operation of 30% and a constant rate of urea injection (45 Hz) until reaching a steady-state condition with minimal levels of NO_x. Then, the rate of urea injection was lowered in steps about every ten minutes from 45 to 40 to 20 Hz, and then finally turned completely off. A commercially available NO_x sensor was located downstream of the prototype. The results are shown in Fig. 6a, which includes a comparison of the prototype sensor response, along with the results from gas analysis using Fourier transform infrared (FTIR) spectroscopy and the commercial sensor signal. In Fig. 6b, the predominant NO_x species measured by FTIR during this portion of engine testing was NO, with very low levels of NO_2 and NH_3 detected. The progressively lower frequency urea injection levels corresponded to smaller amounts of urea in the SCR to react with the NO_x, and therefore resulted in larger concentrations of NO in the exhaust that varied between about 30 to 260 ppm.

Figure 7a shows measurements for O_2, CO_2, H_2O, CO, and CH_4 in the exhaust taken during the same engine testing shown in Fig. 6. These components do not vary significantly over the timescale of the experiment and therefore can not be used to explain changes seen in the measured sensor signal. Figure 7b shows the variation of the temperature during the same engine testing shown

in Fig. 6. As seen in reference to the sensor response in Fig. 6a, there does not appear any correlation between the measured temperature and the measured signal from the NO_x prototype, indicating that the measured signal is fairly tolerant to changes in temperature over this range (about 660 to 670°C).

In the dynamometer engine test cell, the composition of diesel exhaust is influenced by the overall condition of the engine and exhaust after-treatment system, including history and age. The testing results indicated that the dynamometer engine test cell and urea-based SCR were not able to achieve levels of NO_x less than about 30 ppm. The exact requirements for the NO_x sensor will depend on the design of the entire exhaust after-treatment system, which is currently an active area of research and development. However, the most promising technologies being pursued suggest that the sensor will need to detect levels typically less than ∼20 ppm. Based on the bench-level laboratory testing discussed above, the NO_x prototype had better sensitivity at lower concentrations (less than 20 ppm) compared to higher concentrations, as shown in Fig. 4b.

Figure 6a shows that the commercial sensor (blue curve) and FTIR (green curve) measurements track very closely over this concentration range. The prototype response qualitatively parallels the responses obtained for the FTIR and commercial sensor. However, the sensitivity differs, with more pronounced differences at NO concentrations higher than ∼100 ppm. The behavior of the prototype sensor in engine testing appears to show higher sensitivity to NO at lower concentrations, which is in agreement with results from the bench-level laboratory testing (Fig. 4b).

The measured sensor behavior in bench-level laboratory testing was used to adjust the measured phase angle (θ_{meas}) in engine dynamometer testing. The adjustment accounted for the lower sensitivity at high NO concentrations compared with the higher sensitivity at low NO concentrations. The adjusted values for the phase angle signal (θ_{adj}) were calculated using the two different sensitivity values shown in Fig. 4b, given by the two slopes, m_{low} and m_{high}, which are 0.05 and 0.03 deg/ppm NO, respectively. The baseline value for the

adjusted phase angle ($\theta_{baseline}$) was chosen at the initial concentration of ∼30 ppm NO measured from about 80 to 86 min. in Fig. 6, which was approximately −14 deg. The adjusted values are given by the following equations:

$$\theta_{adj} = \theta_{baseline} + \Delta\theta_{adj} \tag{1}$$

$$\Delta\theta_{adj} = \frac{\theta_{meas} - \theta_{baseline}}{\mathrm{m}_{high}}\mathrm{m}_{low} \tag{2}$$

Figure 8 shows the adjusted phase angle signal after accounting for the different sensitivities at low and high NO concentrations. The adjusted phase angle signal has better agreement with both the commercial sensor and FTIR over the entire range of concentrations from 30 to 260 ppm NO compared with the original data shown in Fig. 6a. In Fig. 8, the adjusted sensor signal for ∼150 ppm (from 100 to 110 min), however, did not show as good of agreement, indicating that the linear approximation from bench-level testing fails to completely account for the nonlinear sensitivity over the entire range of concentrations from 30 to 260 ppm NO.

3.3. Engine testing: O_2 cross-sensitivity

Unlike the first protocol discussed above, which minimized interference effects, the second protocol investigated the effect of O_2 cross-senstivity. The engine was again initially operated under a constant throttle operation of 30% and a constant rate of urea injection (45 Hz) until reaching a steady-state condition with minimal levels of NO_x. The level of urea injection was kept constant at 45 Hz during the entire test sequence, while the throttle was increased from the initial 30% to 40%, before stepping to lower levels of 35 to 32.5 to 30%. A commercially available NO_x sensor was located downstream of the prototype.

The results are shown in Fig. 9a, which includes a comparison of the prototype sensor response, along with the results from FTIR gas analysis and the commercial sensor signal. In Fig. 9b, the predominant NO_x species measured by FTIR during this portion of engine testing was NO, with very low levels of NO_2 and NH_3 detected. The initial change in throttle from 30 to 40% at 19

min. corresponded to an abrupt increase in the level of NO to almost 350 ppm. Afterwards, the progressively lower throttle levels to 35, 32.5, and 30%, then corresponded to decreasing amounts of NO, which varied between about 10 and 350 ppm NO over the entire test sequence.

Figure 10a shows measurements for O_2, CO_2, H_2O, CO, and CH_4 in the exhaust taken during the same engine testing shown in Fig. 9. The initial change in throttle from 30 to 40% at 19 min. corresponded to an increase in CO_2 and H_2O, and a decrease in O_2. Subsequent changes to progressively lower throttle levels corresponded to decreasing amounts of CO_2 and H_2O, and increasing amount of O_2. The concentrations of CO and CH_4 remained low and constant during engine testing. Figure 10b shows the variation of the temperature during the same engine testing shown in Fig. 9. As seen in reference to the sensor response in Fig. 9a, there does not appear any correlation between the measured temperature and the measured signal from the NO_x prototype, indicating that the measured signal is fairly tolerant to changes in temperature over this range (about 654 to 661°C).

In Fig. 10a, changes in both CO_2 and H_2O occurred over a 2% range, while changes in O_2 concentration occurred over a range twice as large, from about 5 to 9% (4% range). Bench-level testing indicated that changes in O_2 concentration from 4 to 7% corresponded with a phase angle sensitivity of about 2 deg/% O_2 (see discussion above and Fig. 5). Therefore, in the engine testing using the second protocol, changes in both O_2 and NO_x concentration influenced the measured phase angle signal.

The measured phase angle (θ_{meas}) was adjusted for O_2 interference using the corresponding O_2 concentration directly measured during engine testing, $[O_2]_{meas}$. The phase angle signal adjusted for O_2 interference ($\theta_{O2,adj}$) was calculated using the sensitivity value shown in Fig. 5 for low O_2 concentrations (4 to 7%), which is given by the slope, m_{low}=2 deg/% O_2. A baseline value for the measured O_2 concentration, $[O_2]_{baseline}$, was chosen at the initial concentration of ~9% O_2, measured from about 18 to 20 min., shown in Fig. 10a. The adjusted values are given by the following equations:

$$\theta_{O2,adj} = \theta_{meas} - \Delta\theta_{O2} \tag{3}$$

$$\Delta\theta_{O2} = ([O_2]_{meas} - [O_2]_{baseline})\mathrm{m}_{low} \tag{4}$$

Figure 11a shows the adjusted phase angle signal after accounting for the O_2 interference. The adjusted phase angle signal has slightly better agreement with both the commercial sensor and FTIR compared with the original data shown in Fig. 9a. However, the phase angle signal still shows larger deviations at higher concentrations, greater than ∼100 ppm NO, due to the nonlinear sensitivity behavior.

To account for the different NO sensitivity at low and high concentrations, the phase angle adjusted for O_2 interference ($\theta_{O2,adj}$) was then used in Eqs. 1 and 2, where $\theta_{meas} = \theta_{O2,adj}$. The same sensitivity values were used as before, given by the two slopes in Fig. 4b, m_{low} and m_{high}, which are 0.05 and 0.03 deg/ppm NO, respectively. The baseline value ($\theta_{baseline}$) was chosen as the value for $\theta_{O2,adj}$ at ∼65 ppm NO measured from about 23 to 26 min. in Fig. 9, which was about −8.3 deg.

Figure 11b shows the adjusted phase angle signal after accounting for both the O_2 interference (Fig. 11a) and the different sensitivities at low and high NO concentrations. The adjusted phase angle signal has better agreement with both the commercial sensor and FTIR compared with the data only adjusted for O_2 interference shown in Fig. 11b. However, data at higher NO concentrations greater than ∼100 ppm did not show as good of agreement, again indicating that the linear approximation from bench-level testing fails to completely account for the nonlinear sensitivity over the entire range of concentrations. Furthermore, although changes in both CO_2 and H_2O occurred over a small 2% range, they could also be contributing to the measured phase angle signal.

4. Conclusions

The performance of Au/YSZ/Pt NO_x prototype sensors was evaluated in both bench-level laboratory testing with controlled gas compositions and in dynamometer testing with diesel exhaust. Results in diesel exhaust generally agreed with laboratory testing, which indicated a nonlinear dependence of the NO_x and O_2 sensitivity with concentration. In laboratory testing, the NO_x prototype sensor had higher NO_x and O_2 sensitivity at concentrations less than $\sim$20 ppm and $\sim$7%, respectively, compared to lower NO_x and O_2 sensitivity at concentrations greater than $\sim$50 ppm and $\sim$10.5%, respectively. Diesel exhaust after-treatment systems will likely require detection levels less than $\sim$20 ppm in order to meet emission regulations.

The sensitivity behavior from bench-level laboratory testing was used to adjust the sensor signal from testing in diesel exhaust and account for the nonlinear sensitivity for NO_x and O_2. Adjusted sensor signals had better agreement with both the commercial NO_x sensor and measured gas compositions compared with the original raw sensor signals. However, the lack of complete agreement indicated that the approximation for sensitivity did not completely account for the nonlinear sensor behavior.

Vitae

Leta Woo is a Staff Scientist in the Chemical Sciences Division at Lawrence Livermore National Laboratory. She received her B.S. from Georgia Tech in 2000 and her Ph.D. from Northwestern University in 2005, both in materials science and engineering. Her current research interests include solid-state electrochemical sensors, solid-oxide fuel cells, structure-property relationships in electroceramics and electrocomposites, and electrochemical characterization techniques.

Robert Glass is a Senior Scientist at Lawrence Livermore National Laboratory (LLNL). He is currently leading efforts in solid-state, high temperature elec-

trochemical devices. Dr. Glass is the LLNL Program Lead for the DOE Fuel Cell Technologies Program. He has served as the program manager for efforts in solid oxide fuel cells, high temperature steam electrolysis, and sensors. He is a member of the Executive Committee of the High Temperature Materials Division of The Electrochemical Society. He has over 100 publications and 17 patents. He received his Ph.D. in chemistry from the University of Illinois in 1980.

Robert Novak is a Technical Expert in the Sensors Group in the Chemical Engineering Department, Research and Advanced Engineering, at Ford Motor Company.

Jaco Visser is a Technical Leader in the Sensors Group in the Chemical Engineering Department, Research and Advanced Engineering, at Ford Motor Company.

Acknowledgements

This work was performed under the auspices of the U.S. Department of Energy by Lawrence Livermore National Laboratory under Contract DE-AC52-07NA27344. Two of the coauthors (LYW and RSG) would like to acknowledge support from the DOE Office of Vehicle Technologies and the Program Manager, Jerry Gibbs. We also gratefully acknowledge contributions from Rachel Snow, David Kubinski, and Rick Soltis, all from Ford Motor Company.

References

[1] R. Moos, *Sensors*, **10**, 6773 (2010).

[2] N. Yamazoe, *Sens. Actuators, B*, **108**, 2 (2005).

[3] R. Moos, *Int. J. Appl. Ceram. Technol.*, **2**, 401 (2005).

[4] S. Akbar, P. Dutta, and C. Lee, *Int. J. Appl. Ceram. Technol.*, **3**, 302 (2006).

[5] F. Ménil, V. Coillard, and C. Lucat, *Sens. Actuators, B*, **67**, 1 (2000).

[6] S. Zhuiykov and N. Miura, *Sens. Actuators, B*, **121**, 639 (2007)

[7] J. W. Fergus, *Sens. Actuators, B*, **121**, 652 (2007)

[8] S. -W. Song, L. P. Martin, R. S. Glass, E. P. Murray, J. H. Visser, R. E. Soltis, R. F. Novak, and D. J. Kubinski, *J. Electrochem. Soc.*, **153**, H171 (2006)

[9] N. Miura, M. Nakatou, and S. Zhuiykov, *Ceram. Int.*, **30**, 1135 (2004).

[10] N. Wu, Z. Chen, J. Xu, M. Chyu, and S.X. Mao, *Sens. Actuators, B*, **110**, 49 (2005).

[11] N. Miura, T. Koga, M. Nakatou, P. Elumalai, and M. Hasei, *J. Electroceram.*, **17**, 979 (2006).

[12] L. P. Martin, L. Y. Woo, and R. S. Glass, *J. Electrochem. Soc.*, **154**, J97 (2007).

[13] L. Y. Woo, L. P. Martin, R. S. Glass, and R. J. Gorte, *J. Electrochem. Soc.*, **154**, J129 (2007).

[14] L. Y. Woo, L. P. Martin, R. S. Glass, W. Wang, S. Jung, R. J. Gorte, E. P. Murray, R. F. Novak, and J. H. Visser, *J. Electrochem. Soc.*, **155**, J32 (2008).

[15] L. Y. Woo, R. S. Glass, R. F. Novak, and J. H. Visser, *J. Electrochem. Soc.*, **157**, J81 (2010).

[16] J. R. Macdonald, *Impedance Spectroscopy: Emphasizing Solid Materials and Systems*, p. 5, John Wiley & Sons, New York (1987).

List of Figures

Figure 10. Dynamometer engine testing with constant level of urea injection while stepping throttle (corresponds to Fig. 9): (a) Steady-state values for CO and CH_4 with changes in CO_2, H_2O, and O_2 and (b) variation in temperature.
Figure 11. (a) Phase angle response of Au/YSZ/Pt sensor (red, left y-axis), adjusted for interfering O_2 behavior (see Fig. 5 and text) and (b) also adjusted for behavior at greater than ∼60 ppm NO (see Fig. 4b and text), compared with commercial sensor (blue, right y-axis) and FTIR gas analysis (green, right y-axis); original data shown in Fig. 9a.

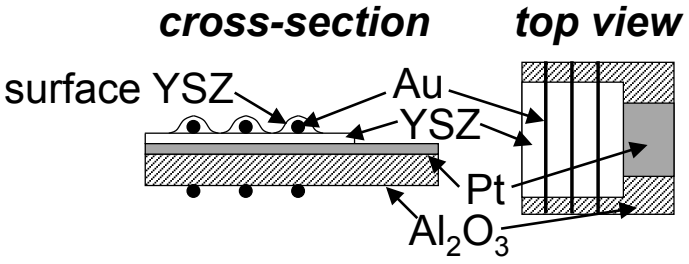

Figure 1: Schematic of Au/YSZ/Pt NO_x sensor prototype.

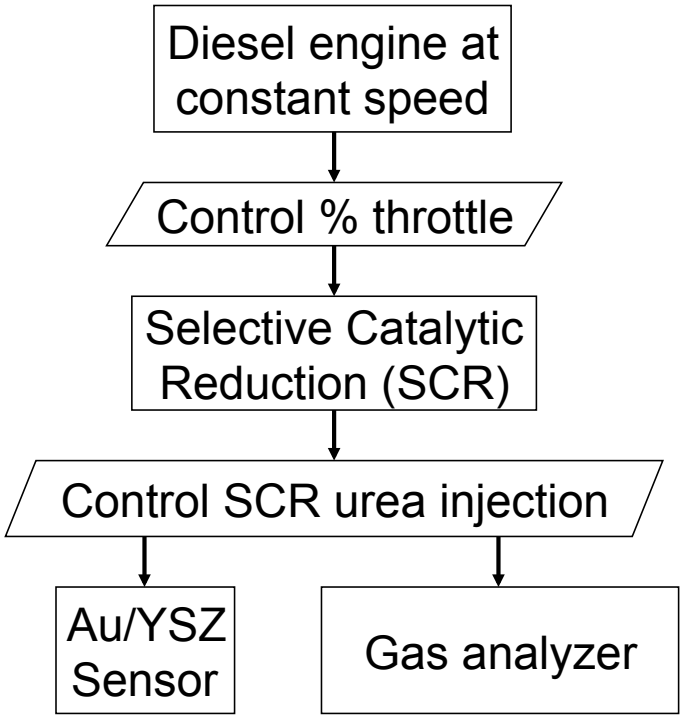

Figure 2: Simplified flow diagram of dynamometer test.

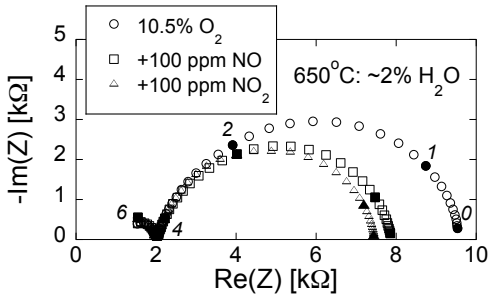

Figure 3: Nyquist plot of Au/YSZ/Pt NO_x sensor prototype in ∼2% H_2O at 650°C in 10.5% O_2 and in 10.5% O_2 with 100 ppm NO or 100 ppm NO_2. Numbers corresponding to darkened points represent log of frequency in Hz.

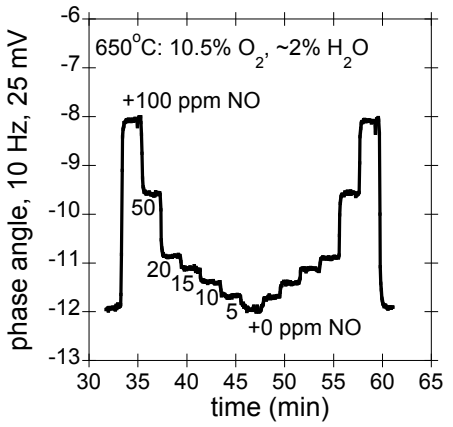

(a)

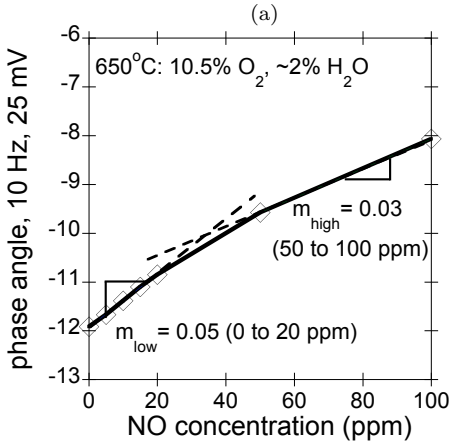

(b)

Figure 4: (a) Phase angle response of Au/YSZ/Pt NO_x sensor prototype stepping in two min. increments through 0-100-50-20-15-10-5-0 ppm NO. (b) Corresponding plot of phase angle signal (deg) vs. NO concentration (ppm) with linear curve fits and calculated slopes (m_{low} and m_{high}) of 0.05 and 0.03 deg/ppm NO for 0 to 20 ppm and for 50 to 100 ppm, respectively.

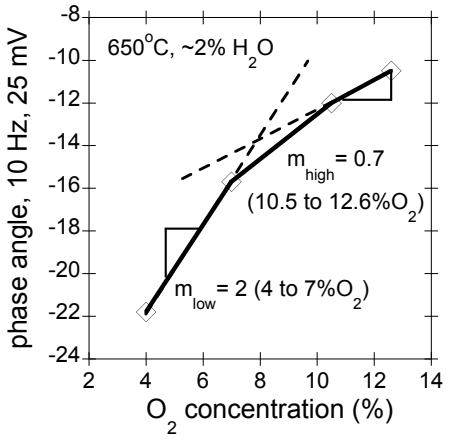

Figure 5: Plot of phase angle signal (deg) vs. O_2 concentration (%), corresponding to laboratory evaluation, with linear curve fits and calculated slopes (m_{low} and m_{high}) of 2 and 0.7 deg/% O_2 for 4 to 7% and for 10.5 to 12.6%, respectively.

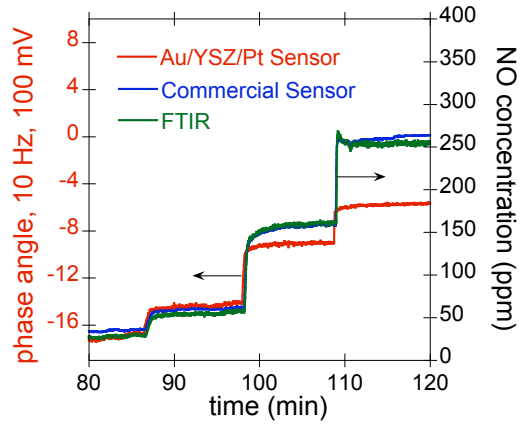

(a)

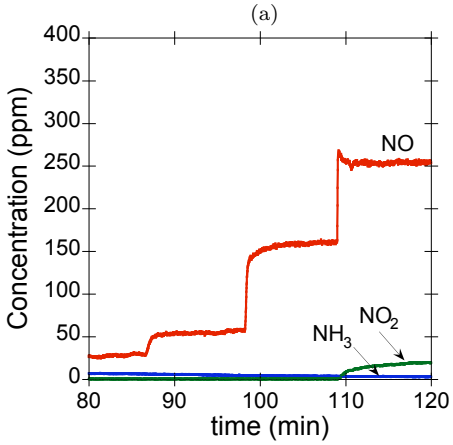

(b)

Figure 6: Dynamometer engine testing with constant throttle while stepping to lower urea injection: (a) Phase angle response of Au/YSZ/Pt sensor (red, left y-axis) compared with a commercial sensor (blue, right y-axis) and FTIR gas analysis (green, right y-axis); (b) FTIR results for NO, NO_2, and NH_3.

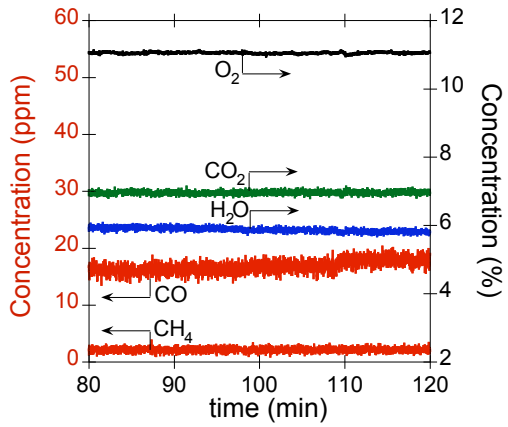

(a)

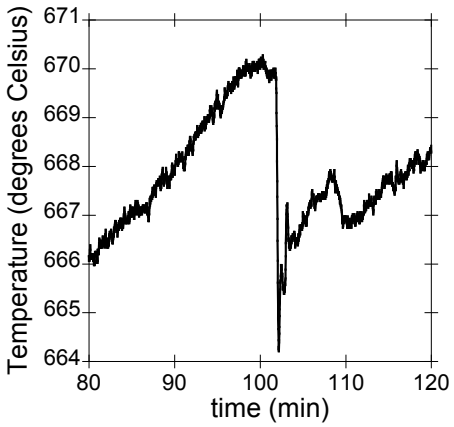

(b)

Figure 7: Dynamometer engine testing with constant throttle while stepping to lower urea injection (corresponds to Fig. 6): (a) Steady-state values for various gases and (b) variation in temperature.

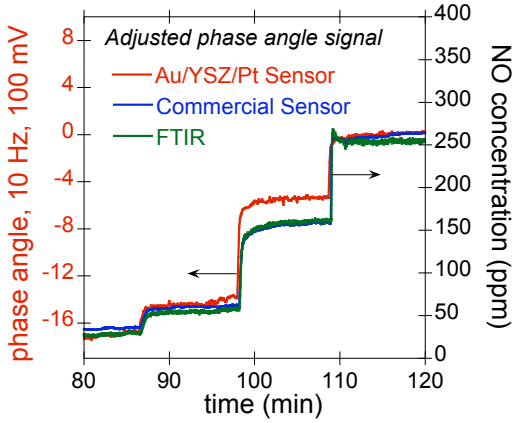

Figure 8: Phase angle response of Au/YSZ/Pt sensor (red, left y-axis), adjusted for behavior at greater than ∼60 ppm NO (see Fig. 4b and text), shows better agreement with a commercial sensor (blue, right y-axis) and FTIR gas analysis (green, right y-axis) compared with original data in Fig. 6a.

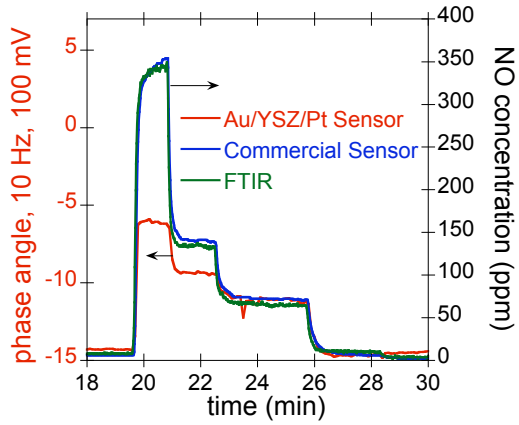

(a)

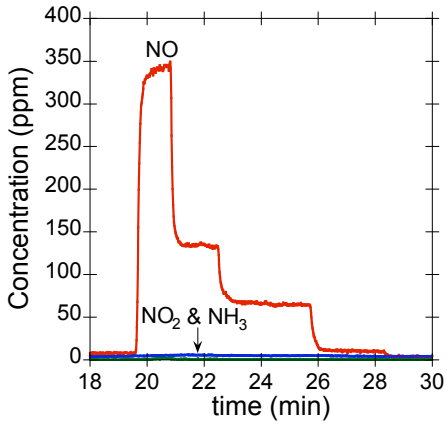

(b)

Figure 9: Dynamometer engine testing with constant level of urea injection while stepping throttle: (a) Phase angle response of Au/YSZ/Pt sensor (red, left y-axis) compared with a commercial sensor (blue, right y-axis) and FTIR gas analysis (green, right y-axis); (b) FTIR results for NO, NO_2, and NH_3.

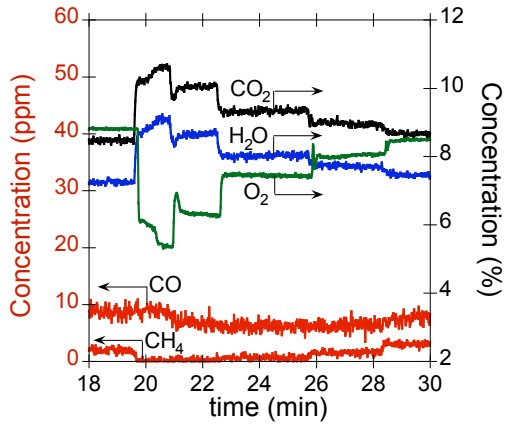

(a)

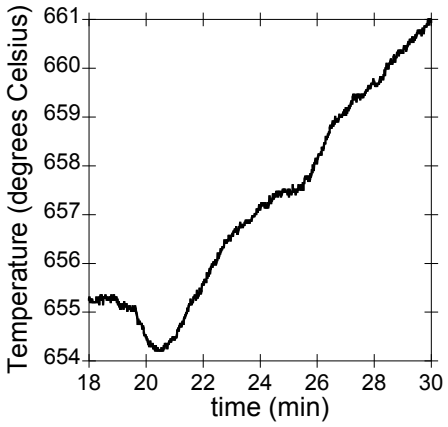

(b)

Figure 10: Dynamometer engine testing with constant level of urea injection while stepping throttle (corresponds to Fig. 9): (a) Steady-state values for CO and CH_4 with changes in CO_2, H_2O, and O_2 and (b) variation in temperature.

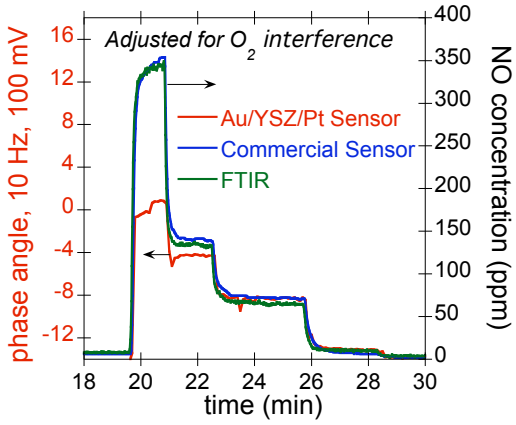

(a)

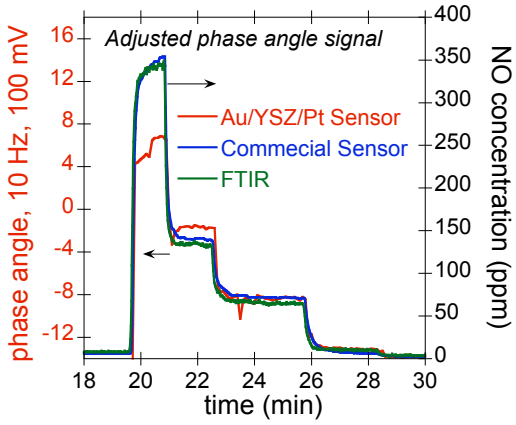

(b)

Figure 11: (a) Phase angle response of Au/YSZ/Pt sensor (red, left y-axis), adjusted for interfering O_2 behavior (see Fig. 5 and text) and (b) also adjusted for behavior at greater than ∼60 ppm NO (see Fig. 4b and text), compared with commercial sensor (blue, right y-axis) and FTIR gas analysis (green, right y-axis); original data shown in Fig. 9a.